electronics

MDPI

Article

Remote-State PWM with Minimum RMS Torque Ripple and Reduced Common-Mode Voltage for Three-Phase VSI-Fed BLAC Motor Drives

Jaehyuk Baik [1], Sangwon Yun [2], Dongsik Kim [3], Chunki Kwon [4] and Jiyoon Yoo [1,*]

1 School of Electrical Engineering, Korea University, 145 Anam-ro, Seongbuk-gu, Seoul 02841, Korea; tyty2000@korea.ac.kr

2 EBS Center of Global R&D, Mando Corporation, 21 Pangyo-ro, Bundang-gu, Seongnam 13486, Korea; sangwon.yun@halla.com

3 Department of Electrical Engineering, Soonchunhyang University, 22 Soonchunhyang-ro, Sinchang-myeon, Asan 31538, Korea; dongsik@sch.ac.kr

4 Department of Medical IT Engineering, Soonchunhyang University, 22 Soonchunhyang-ro, Sinchang-myeon, Asan 31538, Korea; chunkikwon@sch.ac.kr

* Correspondence: jyyoo@korea.ac.kr; Tel.: +82-2-923-9200

Received: 18 March 2020; Accepted: 30 March 2020; Published: 30 March 2020

Abstract: A minimum root mean square (RMS) torque ripple-remote-state pulse-width modulation (MTR-RSPWM) technique is proposed for minimizing the RMS torque ripple under reduced common-mode voltage (CMV) condition of three-phase voltage source inverters (VSI)-fed brushless alternating current (BLAC) motor drives. The q-axis current ripple due to an error voltage vector generated between the reference voltage vector and applied voltage vector is analyzed for all pulse patterns with reduced CMV of the RSPWM. From the analysis result, in the MTR-RSPWM, a sector is divided into five zones, and within each zone, pulse patterns with the lowest RMS torque ripple and reduced CMV are employed. To verify the validity of the MTR-RSPWM, theorical analysis, simulation, and experiments are performed, where the MTR-RSPWM is thoroughly compared with RSPWM3 that generates the minimum RMS current ripple. From the analytical, simulation, and experimental results, it is shown that the MTR-RSPWM significantly reduces the RMS torque ripple under a reduced CMV condition at the expense of an increase in the RMS current ripple, compared to the RSPWM3.

Keywords: common-mode voltage (CMV); reduced common-mode voltage PWM (RCMV-PWM); remote-state PWM (RSPWM); torque ripple; voltage source inverter (VSI)

---

1. Introduction

Nowadays, three-phase voltage-source inverters (VSIs) are widely utilized to control alternating current (AC) motors, and space vector pulse-width modulation (SVPWM) operates inverter switches in order to generate reference voltage [1,2]. However, during SVPWM, an instantaneous error voltage vector is generated between the reference voltage vector and applied voltage vector in the d–q-plane [3–8]. The error voltage vector yields a current ripple vector and it can be decomposed into d–q-axes current ripple vectors, where the q-axis current ripple vector is directly related to the output torque ripple [6–8]. It is known that the error voltage vector is determined mainly by the switching frequency and pulse-width modulation (PWM) technique. However, because the switching frequency cannot be increased beyond a certain range owing to practical limitations, various PWM techniques based on the conventional SVPWM (CSVPWM) have been reported that reduce the error voltage vector, in terms of root mean square (RMS) torque ripple [6–10] and RMS current ripple [3–5].

On the other hand, three-phase VSI-fed AC motor drives also have common-mode voltage (CMV) and common-mode current (CMC) problems. The CMV and the CMC are inevitably generated during the PWM. The high dv/dt of the CMV and corresponding CMC are known to cause electromagnetic interference (EMI), breakdown of winding insulation, bearing failure, and more [11–14]. There are various methods to reduce or eliminate the CMV, such as active/passive filters [11,12], cancellation circuits [13,14], and reduced CMV-PWMs (RCMV-PWMs) [15–25]. Because the RCMV-PWMs do not increase the size of the system and do not incur additional costs, research has now been focused on the development of various RCMV-PWMs. The RCMV-PWMs have also been extended to various inverter-fed motor drives such as the multi-level inverter [21], the dual inverter [22], T-type inverter [23], multi-level matrix converter [24], and more. The RCMV-PWMs for the three-phase VSI-fed AC motor drives can be divided into three groups as the most successful representatives: the active zero state PWM (AZSPWM) [15,16,19,20], the near-state PWM (NSPWM) [18–20], and the remote-state PWM (RSPWM) [19,20]. Their various performances and characteristics, such as output current ripple, modulation index, switching number, CMV magnitude, CMV frequency, and more, are well-researched [19,20].

However, studies on torque performance and its improvement of RCMV-PWMs have not been performed so far. The torque ripple is an important issue that affects the performance of the motors. The torque ripple primarily affects the accuracy of position and speed control systems for brushless alternating current (BLAC) motors, which is pivotal in the applications that require very accurate position and speed control such as robotic systems. Furthermore, the torque ripple induces undesired mechanical vibrations and acoustic noise in the motors [6–8,26,27]. Therefore, minimization of the torque ripple even under reduced CMV conditions is still an important issue.

In this study, among the RCMV-PWMs, the RSPWM that has the most favorable CMV feature is selected to study torque ripple and its minimization [17,19,20]. By extending the previous research on minimizing the RMS torque ripple based on the CSVPWM [6–8], this study proposes minimum RMS torque ripple-remote-state PWM (MTR-RSPWM) for three-phase VSI-fed BLAC motor drives.

This paper is structured as follows. Section 2 introduces the basic concept of the RSPWM reducing the CMV compared to CSVPWM. Section 3 defines the RMS torque ripple and the RMS current ripple over a subcycle by error voltage vector. In Section 4, all pulse patterns of the RSPWM are calculated and analyzed in terms of the RMS torque ripple over a subcycle, and the proposed MTR-RSPWM is described. The RMS torque ripple and the RMS current ripple over a fundamental cycle of the RSPWM3 and MTR-RSPWM are compared in Section 5, where the analytical, simulation, and experimental results are presented and discussed. The conclusions are presented in Section 6.

2. Remote-State PWM

The three-phase VSI-fed BLAC motor drive is shown in Figure 1. In this system, the CMV is defined as the potential difference between the star point of the load and the center of the dc-link of the inverter. From the three-phase balance condition, the CMV can be calculated as follows [15–20]:

$$V_{cm} = V_{no} = (V_{ao} + V_{bo} + V_{co})/3 \tag{1}$$

where V_{ao}, V_{bo}, and V_{co} are the pole voltages of the a, b, and c phases, respectively.

The three-phase VSI has eight switching states, and they can be expressed as voltage vectors in the d–q-plane. Among these voltage vectors, V_0 and V_7 are known as the zero voltage vectors, and the vectors from V_1 to V_6 are known as the active voltage vectors. The pulse patterns of SVPWMs for synthesizing the reference voltage vector are selected based on a specified performance criterion such as the minimum output voltage ripple, switching number, and more. In the space vector approach, the duty cycle of the voltage vectors are calculated according to the vector voltage-seconds balance rule.

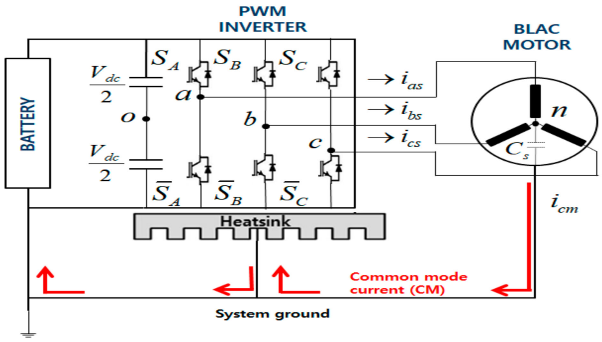

Figure 1. Three-phase voltage source inverter (VSI)-fed brushless alternating current (BLAC) motor drive.

On the other hand, the pulse patterns of SVPWMs are changed by sector in which reference voltage vector is located in the d–q-plane. In general, SVPWMs use A-type or B-type as sector classifiers. The A-type classifies d–q-plane into A_1–A_6 (starting from 0°, defined by an interval of 60°) as shown in Figure 2a–c, and the B-type classifies d–q-plane into B_1–B_6 (starting from −30°, defined by an interval of every 60°) as shown in Figure 2d.

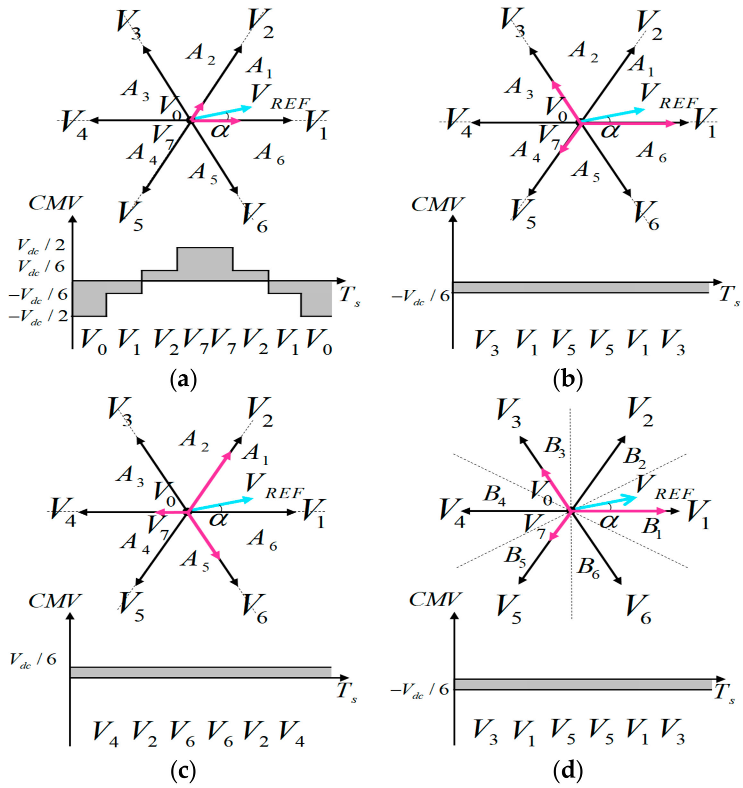

Figure 2. Formation of voltage vectors in the d–q-plane and corresponding common-mode voltage (CMV): (**a**) conventional space vector pulse-width modulation (CSVPWM); (**b**) remote-state pulse-width modulation (RSPWM)1, RSPWM2A; (**c**) RSPWM2B; (**d**) RSPWM3.

Table 1 shows the CMV according to the voltage vectors. Note that the zero voltage vectors generate a large CMV ($-V_{dc}/2$ or $+V_{dc}/2$) and the active voltage vectors generate a small CMV ($-V_{dc}/6$ or $+V_{dc}/6$) [15–20].

Table 1. Inverter Pole Voltage and CMV by Voltage Vector.

Switching State		V_{ao}	V_{bo}	V_{co}	CMV
Zero voltage vector	$V_0(0,0,0)$	$-V_{dc}/2$	$-V_{dc}/2$	$-V_{dc}/2$	$-V_{dc}/2$
	$V_7(1,1,1)$	$+V_{dc}/2$	$+V_{dc}/2$	$+V_{dc}/2$	$+V_{dc}/2$
Active voltage vector	$V_1(1,0,0)$	$+V_{dc}/2$	$-V_{dc}/2$	$-V_{dc}/2$	$-V_{dc}/6$
	$V_2(1,1,0)$	$+V_{dc}/2$	$+V_{dc}/2$	$-V_{dc}/2$	$+V_{dc}/6$
	$V_3(0,1,0)$	$-V_{dc}/2$	$+V_{dc}/2$	$-V_{dc}/2$	$-V_{dc}/6$
	$V_4(0,1,1)$	$-V_{dc}/2$	$+V_{dc}/2$	$+V_{dc}/2$	$+V_{dc}/6$
	$V_5(0,0,1)$	$-V_{dc}/2$	$-V_{dc}/2$	$+V_{dc}/2$	$-V_{dc}/6$
	$V_6(1,0,1)$	$+V_{dc}/2$	$-V_{dc}/2$	$+V_{dc}/2$	$+V_{dc}/6$

The CSVPWM utilizes two active voltage vectors that are adjacent to the reference voltage vector and two zero voltage vectors to synthesize the reference voltage vector. Therefore, the peak value of CMV becomes $\pm V_{dc}/2$. The formation of voltage vectors in sector A_1 ($0° \leq \alpha < 60°$) and corresponding CMV are shown in Figure 2a. The pulse patterns for all sectors are listed in Table 2.

Table 2. Pulse Patterns of the CSVPWM and the RSPWMs.

	A_1	A_2	A_3	A_4	A_5	A_6
CSVPWM	$V_0V_1V_2V_7$ $V_7V_2V_1V_0$	$V_0V_3V_2V_7$ $V_7V_2V_3V_0$	$V_0V_3V_4V_7$ $V_7V_4V_3V_0$	$V_0V_5V_4V_7$ $V_7V_4V_5V_0$	$V_0V_5V_6V_7$ $V_7V_6V_5V_0$	$V_0V_1V_6V_7$ $V_7V_6V_1V_0$
RSPWM1	$V_3V_1V_5$ $V_5V_1V_3$	$V_3V_1V_5$ $V_5V_1V_3$	$V_3V_1V_5$ $V_5V_1V_3$	$V_3V_1V_5$ $V_5V_1V_3$	$V_3V_1V_5$ $V_5V_1V_3$	$V_3V_1V_5$ $V_5V_1V_3$
RSPWM2A	$V_3V_1V_5$ $V_5V_1V_3$	$V_1V_3V_5$ $V_5V_3V_1$	$V_1V_3V_5$ $V_5V_3V_1$	$V_1V_5V_3$ $V_3V_5V_1$	$V_1V_5V_3$ $V_3V_5V_1$	$V_3V_1V_5$ $V_5V_1V_3$
RSPWM2B	$V_4V_2V_6$ $V_6V_2V_4$	$V_4V_2V_6$ $V_6V_2V_4$	$V_2V_4V_6$ $V_6V_4V_2$	$V_2V_4V_6$ $V_6V_4V_2$	$V_2V_6V_4$ $V_4V_6V_2$	$V_2V_6V_4$ $V_4V_6V_2$
	B_1	B_2	B_3	B_4	B_5	B_6
RSPWM3	$V_3V_1V_5$ $V_5V_1V_3$	$V_4V_2V_6$ $V_6V_2V_4$	$V_1V_3V_5$ $V_5V_3V_1$	$V_2V_4V_6$ $V_6V_4V_2$	$V_1V_5V_3$ $V_3V_5V_1$	$V_2V_6V_4$ $V_4V_6V_2$

However, the RSPWMs utilize three active voltage vectors that are 120° apart from each other (remote-state vectors) to synthesize the reference voltage vector. There are two types of pulse patterns, yielding a total of six pulse patterns: (1) the odd pulse patterns consist of three odd active voltage vectors, i.e., $V_1V_3V_5V_5V_3V_1$, $V_1V_5V_3V_3V_5V_1$, and $V_3V_1V_5V_5V_1V_3$, and (2) the even pulse patterns consist of three even active voltage vectors, i.e., $V_2V_4V_6V_6V_4V_2$, $V_2V_6V_4V_4V_6V_2$, and $V_4V_2V_6V_6V_2V_4$. During switching period, the odd pulse patterns generate constant CMV of $-V_{dc}/6$, and even pulse patterns generate constant CMV of $+V_{dc}/6$. The RSPWM1 utilizes only one pulse pattern. One of the six pulse patterns for all sectors is listed in Table 2 and its formation of voltage vectors in sector A_1 and corresponding CMV are shown in Figure 2b. The RSPWM2 utilizes only one type of pulse pattern, i.e., the odd pulse patterns or the even pulse patterns. The RSPWM2A utilizes odd pulse patterns and the RSPWM2B utilizes even pulse patterns. Their pulse patterns for all sectors are listed in Table 2. The formations of voltage vectors in sector A_1 and corresponding CMVs are shown in Figure 2b,c, respectively. The RSPWM3 utilizes all six pulse patterns as listed in Table 2. Its formation of voltage vectors in sector B_1 ($-30° \leq \alpha < 30°$) and corresponding CMV is shown in Figure 2d. As listed in Table 2, the pulse patterns for all sectors of RSPWMs are different. Thus, the overall performances and characteristics over a fundamental cycle are different for each sector [19,20], when compared with the CSVPWM that was sufficiently studied. However, all RSPWMs reduce the peak value of the CMV to $\pm V_{dc}/6$, corresponding to a third of that of CSVPWM. Moreover, the CMVs are maintained at a constant value during 60° (RSPWM3) or 360° (RSPWM1, RSPWM2A, RSPWM2B).

Utilizing the pulse patterns of RSPWMs defined above, the PWM period equation and the complex variable voltage-seconds balance equation for RSPWMs can be written in a generalized form as follows:

$$\mathrm{V_{i+1}T_{i+1} + V_{i+3}T_{i+3} + V_{i+5}T_{i+5} = V_{REF}T_s} \tag{2}$$

$$\mathrm{T_{i+1} + T_{i+3} + T_{i+5} = T_s,\ i \in \{0, 1\}} \tag{3}$$

where $\mathrm{V_i}$ is voltage vector, $\mathrm{T_i}$ is applied time of voltage vector, $\mathrm{T_s}$ is switching period, and $\mathrm{V_{REF}}$ is amplitude of reference voltage vector. Normalizing the voltage vector on-time values with $2\mathrm{V_{dc}}/3$, and using (2) and (3), applied time of voltage vectors for the two types of pulse patterns can be calculated as follows:

$$\mathrm{T_1} = (\frac{1}{3} + \frac{2}{\pi}\mathrm{M_i}\cos\alpha)\mathrm{T_s} \tag{4a}$$

$$\mathrm{T_3} = (\frac{1}{3} - \frac{1}{\pi}\mathrm{M_i}\cos\alpha + \frac{\sqrt{3}}{\pi}\mathrm{M_i}\sin\alpha)\mathrm{T_s} \tag{4b}$$

$$\mathrm{T_5} = (\frac{1}{3} - \frac{1}{\pi}\mathrm{M_i}\cos\alpha - \frac{\sqrt{3}}{\pi}\mathrm{M_i}\sin\alpha)\mathrm{T_s} \tag{4c}$$

$$\mathrm{T_2} = (\frac{1}{3} + \frac{1}{\pi}\mathrm{M_i}\cos\alpha + \frac{\sqrt{3}}{\pi}\mathrm{M_i}\sin\alpha)\mathrm{T_s} \tag{5a}$$

$$\mathrm{T_4} = (\frac{1}{3} - \frac{2}{\pi}\mathrm{M_i}\cos\alpha)\mathrm{T_s} \tag{5b}$$

$$\mathrm{T_6} = (\frac{1}{3} + \frac{1}{\pi}\mathrm{M_i}\cos\alpha - \frac{\sqrt{3}}{\pi}\mathrm{M_i}\sin\alpha)\mathrm{T_s} \tag{5c}$$

where α is the angle of $\mathrm{V_{REF}}$, and the modulation index $\mathrm{M_i}$ (voltage utilization level) is defined as follows:

$$\mathrm{M_i = V_{s1}/V_{s1,6\text{-}step}} \tag{6}$$

where $\mathrm{V_{s1,\,6\text{-}step}} = 2\mathrm{V_{dc}}/\pi$, $\mathrm{V_{s1}}$ is the magnitude of the fundamental component of $\mathrm{V_{REF}}$ and $\mathrm{V_{dc}}$ is the input dc voltage of inverter.

3. Analysis of Torque and Current Ripple

As described in the previous section, RSPWM has a total of six pulse patterns. They can synthesize the same reference voltage vector, on average. However, there is an instantaneous error voltage vector between the reference voltage vector and applied active voltage vector. Thus, error voltage vectors generated by each pulse pattern over a subcycle are different from each other. For a given reference voltage vector as an example, the error voltage vectors corresponding to the six active voltage vectors are as illustrated in Figure 3, and can be expressed as follows:

$$\mathrm{V_{ERROR,i} = V_i - V_{REF},\ i \in \{1, \ldots, 6\}} \tag{7}$$

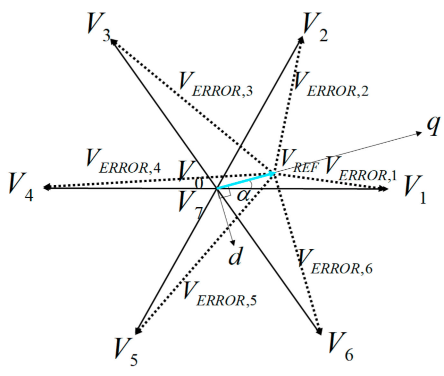

Figure 3. Error voltage vectors in the d–q-plane.

Since the error voltage vector sees the motor as its total leakage inductance, the current ripple vector is proportional to the time integral of the error voltage vector. The current ripple vector can be decomposed into d–q-axes current ripple vectors. When the q-axis is the reference axis of a synchronously revolving reference frame and the reference voltage vector is aligned with the q-axis as shown in Figure 3, the trajectory of the error vectors and corresponding d–q-axes current ripple vectors of six pulse patterns of RSPWM are illustrated in Figure 4, where the quantities Q_1–Q_6 and D_1–D_6 are as defined in (8) and (9). These values are products of a component of the error voltage vector corresponding to the applied active voltage vector and its applied time [3–8].

$$Q_1 = (\frac{2}{3}\cos\alpha - \frac{2}{\pi}M_i)T_1\frac{V_{dc}}{l} \quad D_1 = \frac{2}{3}(\sin\alpha)T_1\frac{V_{dc}}{l} \tag{8a}$$

$$Q_3 = (\frac{2}{3}(\cos(60^\circ+\alpha)) - \frac{2}{\pi}M_i)T_3\frac{V_{dc}}{l} \quad D_3 = -\frac{2}{3}((\sin(60^\circ+\alpha))T_3\frac{V_{dc}}{l} \tag{8b}$$

$$Q_5 = (-\frac{2}{3}(\cos(60^\circ-\alpha)) - \frac{2}{\pi}M_i)T_5\frac{V_{dc}}{l} \quad D_5 = \frac{2}{3}((\sin(60^\circ-\alpha))T_5\frac{V_{dc}}{l} \tag{8c}$$

$$Q_2 = (\frac{2}{3}(\cos(60^\circ-\alpha)) - \frac{2}{\pi}M_i)T_2\frac{V_{dc}}{l} \quad D_2 = -\frac{2}{3}((\sin(60^\circ-\alpha))T_2\frac{V_{dc}}{l} \tag{9a}$$

$$Q_4 = (-\frac{2}{3}(\cos\alpha) - \frac{2}{\pi}M_i)T_4\frac{V_{dc}}{l} \quad D_4 = -\frac{2}{3}(\sin\alpha)T_4\frac{V_{dc}}{l} \tag{9b}$$

$$Q_6 = (\frac{2}{3}(\cos(60^\circ+\alpha)) - \frac{2}{\pi}M_i)T_6\frac{V_{dc}}{l} \quad D_6 = \frac{2}{3}((\sin(60^\circ+\alpha))T_6\frac{V_{dc}}{l} \tag{9c}$$

where V_{dc} is the input dc voltage of inverter, M_i is the modulation index, α is the angle of V_{REF}, l is the total leakage inductance of the motor, and T_1–T_6 are the dwell times of V_1–V_6. From the equations, it is observed that the direction of error voltage vector determines the slope of the current ripple trajectory, and the dwell time of the active voltage vector determines the magnitude of the current ripple.

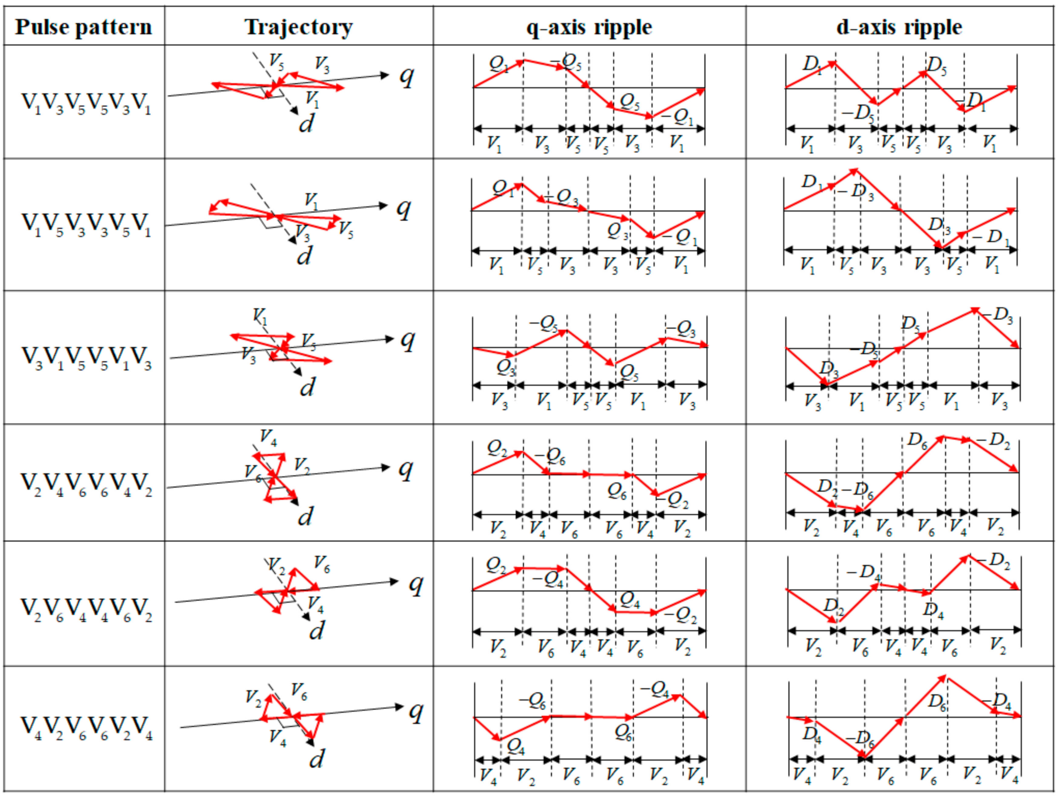

Figure 4. Trajectory of error voltage vector by six pulse patterns of RSPWM and corresponding d–q-axes current ripples.

3.1. RMS Torque Ripple

Under the assumptions that the eddy currents and hysteresis losses are negligible and the iron core of the BLAC motor is unsaturated, the stator d–q-axes voltage equation of the BLAC motor in the synchronous rotating reference frame can be expressed as follows:

$$u_d = Ri_d + \frac{d\lambda_d}{dt} - \omega_r \lambda_q \tag{10a}$$

$$u_q = Ri_q + \frac{d\lambda_q}{dt} + \omega_r \lambda_d \tag{10b}$$

where $\lambda_d = L_d i_d + \lambda_{PM}$ and $\lambda_q = L_q i_q$ are the total flux linkages along the d–q-axes, respectively, λ_{PM} is the permanent magnet flux linkage, ω_r is the mechanical angular speed, u_d and u_q are the stator voltages along the d–q-axes, respectively, i_d and i_q are the stator currents along the d–q-axes, respectively, L_d and L_q are the stator inductances along the d–q-axes, respectively, and R is the stator resistance. In case the rotor of the BLAC motor is surface-mounted, L_d and L_q are equal. Since the reference voltage vector is aligned with the q-axis as shown in Figure 3, the PM flux exists only along the d-axis. Hence, the torque ripple content is generated by interaction between the PM flux and the q-axis current ripple while the d-axis current ripple is responsible for the ripple in the flux linkage in the air gap. The instantaneous torque ripple can be expressed as follows [6–8]:

$$\widetilde{\tau} = \frac{3}{2}P(\lambda_d \widetilde{i}_q - \lambda_q \widetilde{i}_d) = \frac{3}{2}P\lambda_{PM}\widetilde{i}_q = K_T \widetilde{i}_q \tag{11}$$

where K_T is the torque coefficient, P is the number of pole pairs, $\widetilde{i}_d$ and $\widetilde{i}_q$ are the current ripples along the d–q-axes. According to (11), the torque ripple can be seen to be directly proportional to the q-axis current ripple. The RMS torque ripple and the RMS q-axis current ripple over a subcycle can be expressed as follows [6–8]:

$$\widetilde{\tau}_{rms,sub} = K_T \widetilde{i}_{q,rms,sub} \tag{12}$$

$$\widetilde{i}_{q,rms,sub} = \left[\frac{1}{T_s} \int_0^{T_s} \widetilde{i}_q^2 dt \right]^{1/2} \tag{13}$$

Thus, the RMS q-axis current ripples over a subcycle of six pulse patterns of RSPWM in Figure 4 can be calculated using (8), (9), and (13) as follows:

$$\begin{aligned}
\widetilde{i}_{q,rms,sub}^{V_1V_3V_5V_5V_3V_1} &= \sqrt{\tfrac{1}{T_s}\int_0^{T_s} \widetilde{i}_q^2(t)dt} = \sqrt{\tfrac{1}{T_s}\int_0^{T_1}\left(\tfrac{Q_1 t}{T_1}\right)^2 dt + \tfrac{1}{T_s}\int_0^{T_3}\left(Q_1 - \tfrac{(Q_5+Q_1)t_a}{T_3}\right)^2 dt_a + \tfrac{1}{T_s}\int_0^{T_5}\left(-Q_5 + \tfrac{Q_5 t_b}{T_5}\right)^2 dt_b} \\
&= \sqrt{\tfrac{1}{3}Q_1^2\tfrac{T_1}{T_s} + \tfrac{1}{3}\left(Q_1^2 - Q_1Q_5 + (-Q_5)^2\right)\tfrac{T_3}{T_s} + \tfrac{1}{3}(-Q_5)^2\tfrac{T_5}{T_s}} \\
\widetilde{i}_{q,rms,sub}^{V_1V_5V_3V_3V_5V_1} &= \sqrt{\tfrac{1}{3}Q_1^2\tfrac{T_1}{T_s} + \tfrac{1}{3}(Q_1^2 - Q_1Q_3 + (-Q_3)^2)\tfrac{T_5}{T_s} + \tfrac{1}{3}(-Q_3)^2\tfrac{T_3}{T_s}} \\
\widetilde{i}_{q,rms,sub}^{V_3V_1V_5V_5V_1V_3} &= \sqrt{\tfrac{1}{3}Q_3^2\tfrac{T_3}{T_s} + \tfrac{1}{3}(Q_3^2 - Q_3Q_5 + (-Q_5)^2)\tfrac{T_1}{T_s} + \tfrac{1}{3}(-Q_5)^2\tfrac{T_5}{T_s}} \\
\widetilde{i}_{q,rms,sub}^{V_2V_4V_6V_6V_4V_2} &= \sqrt{\tfrac{1}{3}Q_2^2\tfrac{T_2}{T_s} + \tfrac{1}{3}(Q_2^2 - Q_2Q_6 + (-Q_6)^2)\tfrac{T_4}{T_s} + \tfrac{1}{3}(-Q_6)^2\tfrac{T_6}{T_s}} \\
\widetilde{i}_{q,rms,sub}^{V_2V_6V_4V_4V_6V_2} &= \sqrt{\tfrac{1}{3}Q_2^2\tfrac{T_2}{T_s} + \tfrac{1}{3}(Q_2^2 - Q_2Q_4 + (-Q_4)^2)\tfrac{T_6}{T_s} + \tfrac{1}{3}(-Q_4)^2\tfrac{T_4}{T_s}} \\
\widetilde{i}_{q,rms,sub}^{V_4V_2V_6V_6V_2V_4} &= \sqrt{\tfrac{1}{3}Q_4^2\tfrac{T_4}{T_s} + \tfrac{1}{3}(Q_4^2 - Q_4Q_6 + (-Q_6)^2)\tfrac{T_2}{T_s} + \tfrac{1}{3}(-Q_6)^2\tfrac{T_6}{T_s}}
\end{aligned} \tag{14}$$

Thus, the RMS torque ripples over a subcycle of six pulse patterns of RSPWM can be obtained using (12) and (14).

3.2. RMS Current Ripple

Similarly, the RMS *d*-axis current ripple over a subcycle can be expressed as follows [3–5]:

$$\tilde{i}_{d,rms,sub} = \left[\frac{1}{T_s} \int_0^{T_s} \tilde{i}_d^2 dt \right]^{1/2} \tag{15}$$

and the RMS d-axis current ripples over a subcycle of six pulse patterns of RSPWM in Figure 4 can be calculated using (8), (9), and (15) as follows:

$$\begin{aligned}
\tilde{i}_{d,rms,sub}^{V_1V_3V_5V_5V_3V_1} &= \sqrt{\frac{1}{T_s}\int_0^{T_s} \tilde{i}_d^2(t)dt} = \sqrt{\frac{1}{T_s}\int_0^{T_1}\left(\frac{D_1 t}{T_1}\right)^2 dt + \frac{1}{T_s}\int_0^{T_3}\left(D_1 - \frac{(D_5+D_1)t_a}{T_3}\right)^2 dt_a + \frac{1}{T_s}\int_0^{T_5}\left(-D_5 + \frac{D_5 t_b}{T_5}\right)^2 dt_b} \\
&= \sqrt{\frac{1}{3}D_1^2\frac{T_1}{T_s} + \frac{1}{3}\left(D_1^2 - D_1D_5 + (-D_5)^2\right)\frac{T_3}{T_s} + \frac{1}{3}(-D_5)^2\frac{T_5}{T_s}} \\
\tilde{i}_{d,rms,sub}^{V_1V_5V_3V_3V_5V_1} &= \sqrt{\frac{1}{3}D_1^2\frac{T_1}{T_s} + \frac{1}{3}(D_1^2 - D_1D_3 + (-D_3)^2)\frac{T_5}{T_s} + \frac{1}{3}(-D_3)^2\frac{T_3}{T_s}} \\
\tilde{i}_{d,rms,sub}^{V_3V_1V_5V_5V_1V_3} &= \sqrt{\frac{1}{3}D_3^2\frac{T_3}{T_s} + \frac{1}{3}(D_3^2 - D_3D_5 + (-D_5)^2)\frac{T_1}{T_s} + \frac{1}{3}(-D_5)^2\frac{T_5}{T_s}} \\
\tilde{i}_{d,rms,sub}^{V_2V_4V_6V_6V_4V_2} &= \sqrt{\frac{1}{3}D_2^2\frac{T_2}{T_s} + \frac{1}{3}(D_2^2 - D_2D_6 + (-D_6)^2)\frac{T_4}{T_s} + \frac{1}{3}(-D_6)^2\frac{T_6}{T_s}} \\
\tilde{i}_{d,rms,sub}^{V_2V_6V_4V_4V_6V_2} &= \sqrt{\frac{1}{3}D_2^2\frac{T_2}{T_s} + \frac{1}{3}(D_2^2 - D_2D_4 + (-D_4)^2)\frac{T_6}{T_s} + \frac{1}{3}(-D_4)^2\frac{T_4}{T_s}} \\
\tilde{i}_{d,rms,sub}^{V_4V_2V_6V_6V_2V_4} &= \sqrt{\frac{1}{3}D_4^2\frac{T_4}{T_s} + \frac{1}{3}(D_4^2 - D_4D_6 + (-D_6)^2)\frac{T_2}{T_s} + \frac{1}{3}(-D_6)^2\frac{T_6}{T_s}}
\end{aligned} \tag{16}$$

Additionally, the RMS current ripple over a subcycle can be calculated as follows:

$$\tilde{i}_{rms,sub} = \sqrt{\tilde{i}_{q,rms,sub}^2 + \tilde{i}_{d,rms,sub}^2} \tag{17}$$

Thus, using (14), (16), and (17), the rms current ripple over a subcycle of six pulse patterns of RSPWM can be obtained. From the equations, it can be observed that the values of the RMS torque ripple and the RMS current ripple are proportional to the (18a) and (18b), respectively.

$$\tilde{\tau}_{base} = \frac{V_{dc}T_s}{l}K_T \tag{18a}$$

$$\tilde{i}_{base} = \frac{V_{dc}T_s}{l} \tag{18b}$$

Hence, being independent of input dc voltage, switching frequency, and machine parameters, the RMS torque ripple and the RMS current ripple can be normalized with respect to (18a) and (18b), respectively [6–8].

4. Minimum rms Torque Ripple-RSPWM

As described in the previous section, error voltage vectors generated by a pulse pattern determine d–q-axes current ripples, where only the q-axis current ripple is related to the RMS torque ripple. On the other hand, the angle of the reference voltage vector α changes with every subcycle, and the magnitude of the reference voltage vector V_{REF} also changes during variable speed control. Thus, the RMS torque ripple and the RMS current ripple also change every subcycle according to α and M_i ($\propto V_{REF}$). Hence, the RMS torque ripple and the RMS current ripple of the six pulse patterns of RSPWM need to be calculated and analyzed under all ranges of the reference voltage vector (α and M_i).

Figure 5 shows the analytical results of the RMS torque ripple over a subcycle of six pulse patterns of RSPWM under sector B_1 ($-30° \leq \alpha < 30°$) and $0 \leq M_i < 0.52$, that is, the modulation index range of the RSPWM. The RMS torque ripple is calculated using (12)–(14) and normalized by (18a). From Figure 5, it is confirmed that the RMS torque ripple depends on α and M_i, and each pulse pattern has its own RMS torque ripple characteristics. Additionally, it is observed that the pulse pattern with the lowest RMS torque ripple varies with α and M_i in a sector. The comparison shows that the RMS torque ripple corresponding to pulse pattern $V_3V_1V_5V_5V_1V_3$ is the lowest when the reference voltage vector is in Zone 1 and Zone 3 as shown in Figure 6, where $\alpha_{1,1}$ and $\alpha_{2,1}$ are boundary values of α in the sector

B_1, and M_{i1} and M_{i2} are boundary values of M_i. The M_i can also be defined as low M_i when $M_i \leq 0.22$ or high M_i when $M_i > 0.22$. Note that Zones 1 and 3, and Zones 4 and 5 are symmetric around the middle of the sector (i.e., $\alpha = 0°$). Pulse pattern $V_2V_4V_6V_6V_4V_2$, $V_2V_6V_4V_4V_6V_2$ and $V_4V_2V_6V_6V_2V_4$ are best in terms of the RMS torque ripple in Zone 2, Zone 4, and Zone 5, respectively, in Figure 6.

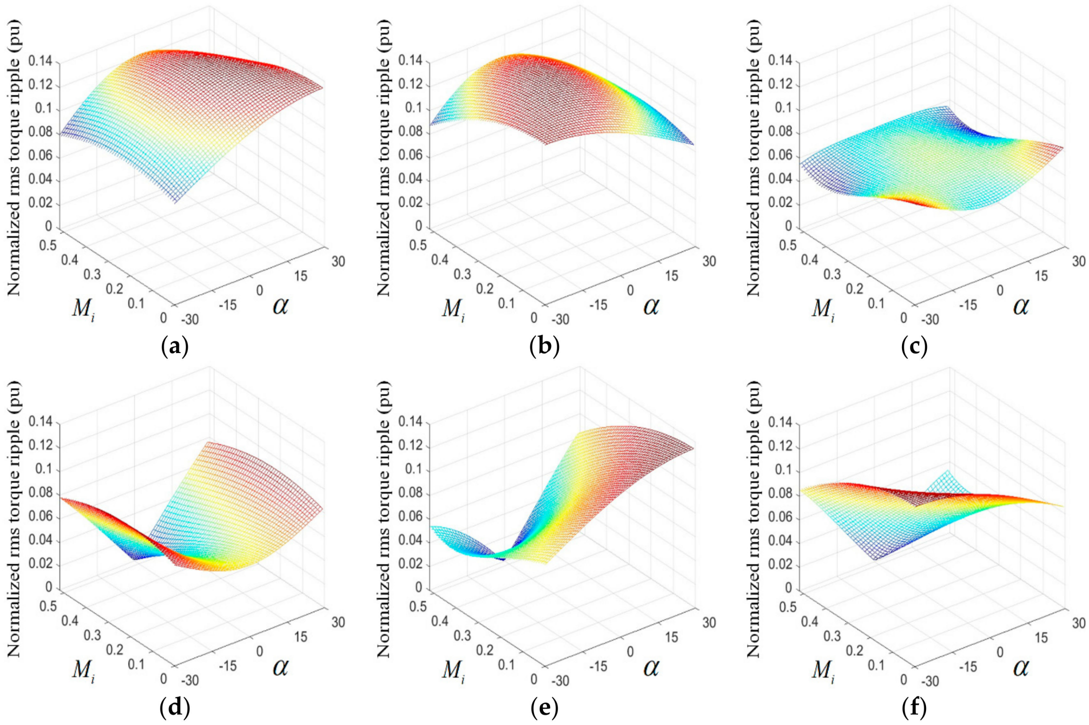

Figure 5. Analytical results of normalized root mean square (RMS) torque ripple over a subcycle. (**a**) $V_1V_3V_5V_5V_3V_1$; (**b**) $V_1V_5V_3V_3V_5V_1$; (**c**) $V_3V_1V_5V_5V_1V_3$; (**d**) $V_2V_4V_6V_6V_4V_2$; (**e**) $V_2V_6V_4V_4V_6V_2$; (**f**) $V_4V_2V_6V_6V_2V_4$.

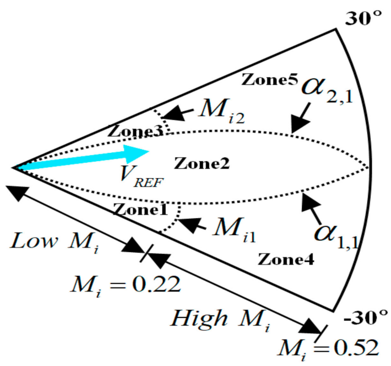

Figure 6. Definition of zone for a minimum root mean square torque ripple-remote-state pulse-width modulation (MTR-RSPWM).

In this way, pulse patterns with zones for sector B_2–B_6 can be obtained, listed in Table 3. Therefore, the proposed RSPWM technique, referred to as MTR-RSPWM, divides each sector into five zones, as shown in Figure 6, and employs pulse patterns with the lowest RMS torque ripple within each zone.

Figure 7 shows a block diagram of the MTR-RSPWM. The look-up table obtained from analytical results receives sector information from sector calculator and outputs the boundary values of α ($\alpha_{1,i}$ and $\alpha_{2,i}$) and M_i (M_{i1} and M_{i2}) corresponding to each sector. After comparing current α and M_i with the boundary values, the zone is determined, and the corresponding pulse pattern is generated by PWM signal generator. The $\alpha_{1,i}$ and $\alpha_{2,i}$ can be obtained as follows:

$$\alpha_{1,i} = \alpha_{1,1} + 60(i-1),$$
$$\alpha_{2,i} = \alpha_{2,1} + 60(i-1) \tag{19}$$

where $\alpha_{1,1}$ and $\alpha_{2,1}$ are the boundary values of α_1 and α_2 in sector B_1, respectively, and i is the number of sector. M_{i1} and M_{i2} for all sectors are same.

Table 3. Pulse Patterns of the MTR-RSPWM.

MTR-RSPWM					
Sector	**Zone 1**	**Zone 2**	**Zone 3**	**Zone 4**	**Zone 5**
B_1	$V_3V_1V_5$ $V_5V_1V_3$	$V_2V_4V_6$ $V_6V_4V_2$	$V_3V_1V_5$ $V_5V_1V_3$	$V_2V_6V_4$ $V_4V_6V_2$	$V_4V_2V_6$ $V_6V_2V_4$
B_2	$V_4V_2V_6$ $V_6V_2V_4$	$V_1V_5V_3$ $V_3V_5V_1$	$V_4V_2V_6$ $V_6V_2V_4$	$V_3V_1V_5$ $V_5V_1V_3$	$V_1V_3V_5$ $V_5V_3V_1$
B_3	$V_1V_3V_5$ $V_5V_3V_1$	$V_2V_6V_4$ $V_4V_6V_2$	$V_1V_3V_5$ $V_5V_3V_1$	$V_4V_2V_6$ $V_6V_2V_4$	$V_2V_4V_6$ $V_6V_4V_2$
B_4	$V_2V_4V_6$ $V_6V_4V_2$	$V_3V_1V_5$ $V_5V_1V_3$	$V_2V_4V_6$ $V_6V_4V_2$	$V_1V_3V_5$ $V_5V_3V_1$	$V_1V_5V_3$ $V_3V_5V_1$
B_5	$V_1V_5V_3$ $V_3V_5V_1$	$V_4V_2V_6$ $V_6V_2V_4$	$V_1V_5V_3$ $V_3V_5V_1$	$V_2V_4V_6$ $V_6V_4V_2$	$V_2V_6V_4$ $V_4V_6V_2$
B_6	$V_2V_6V_4$ $V_4V_6V_2$	$V_1V_3V_5$ $V_5V_3V_1$	$V_2V_6V_4$ $V_4V_6V_2$	$V_1V_5V_3$ $V_3V_5V_1$	$V_3V_1V_5$ $V_5V_1V_3$

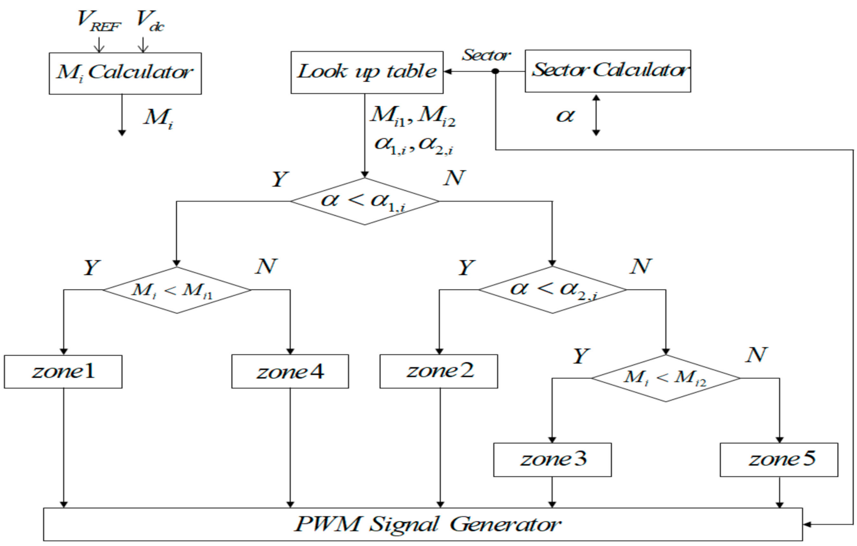

Figure 7. Block diagram of the MTR-RSPWM.

On the other hand, the RMS current ripple over a subcycle is also calculated and analyzed. It is observed that the RMS current ripple, which corresponds to a single pulse pattern, i.e., $V_3V_1V_5V_5V_1V_3$ is the lowest when the reference voltage vector is in sector B_1, for all range of α and M_i. Through further analysis of the other sectors, it is confirmed that obtained pulse patterns are the same as that of RSPWM3 introduced in [19,20]. Hence, the analytical results of normalized RMS current ripple over a subcycle for six pulse patterns are not included in this paper.

From the analysis of six pulse patterns of RSPWM in terms of the RMS torque ripple and RMS current ripple, it is confirmed that minimum RMS torque ripple can be obtained by MTR-RSPWM and minimum RMS current ripple can be obtained by RSPWM3.

5. Results and Discussion

In this section, the analytical, simulation, and experimental results are presented. The analysis and simulation was carried out using MATLAB-R2015b and PSIM-9.0. The experimental setup, based on MCU (TRICORE277, INFINEON), is shown in Figure 8.

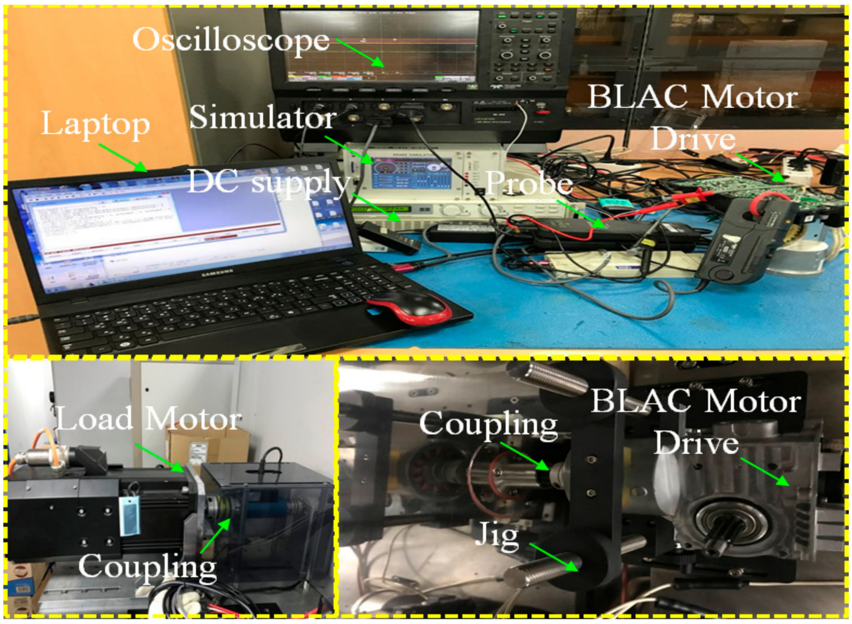

Figure 8. Experimental setup.

The system parameters are listed in Table 4. The test was performed at 500 RPM with $T_L = 0.44$ N·m, corresponding to $M_i = 0.2$. The experimental waveforms were obtained using an oscilloscope (MDA810A, LECROY) and torque performance tester (ADCSYSTEM).

Table 4. System Parameters.

Parameters	Values
DC power supply	12 [V]
Switching frequency	20 [kHz]
Dead time	66 [ns]
Stator resistance	19.6 [mΩ]
Stator inductance	69.9 [μH]
Number of pole pairs	4
Rotor inertia	39.8×10^{-6} [kg·m^2]
Rated speed	1700 [r/min]
Rated torque	1.98 [N·m]
Rated power	0.35 [kW]

In the previous section, the RMS torque ripple and current ripple over a subcycle are calculated for six pulse pattern of RSPWM. These quantities can be averaged over a fundamental cycle to obtain the respective RMS values, as follows [3–8]:

$$\widetilde{i}_{rms,fund} = \left[\frac{1}{2\pi} \int_0^{2\pi} \widetilde{i}^2_{rms,sub} d\alpha \right]^{1/2} \tag{20}$$

$$\widetilde{\tau}_{\text{rms,fund}} = \left[\frac{1}{2\pi} \int_{0}^{2\pi} \widetilde{\tau}^{2}_{\text{rms,sub}} \mathrm{d}\alpha \right]^{1/2} \tag{21}$$

The RMS current ripple and torque ripple over a fundamental cycle by the MTR-RSPWM is evaluated and compared against those of the RSPWM3, which generates minimum RMS current ripple. Figure 9a,b shows the analytical and simulation results of the normalized RMS torque ripple and current ripple over a fundamental cycle corresponding to the RSPWM3 and MTR-RSPWM for M_i ranging from 0 to 0.52 in steps of 0.02. It can be observed that the analytical and simulation results agree well in both the RMS torque ripple and current ripple. The MTR-RSPWM reduces RMS torque ripple compared to the RSPWM3 over the entire range of modulation index, as shown in Figure 9a. The optimum reduction is observed at M_i = 0.44, where the RMS torque ripple is reduced by approximately 50%. On the other hand, MTR-RSPWM increases RMS current ripple compared to RSPWM3 over the entire range of modulation index, as shown in Figure 9b. This phenomenon occurs because the reduction of q-axis current ripple resulted in an increase of d-axis current ripple and the change of d-axis current ripple is greater than that of the q-axis current ripple.

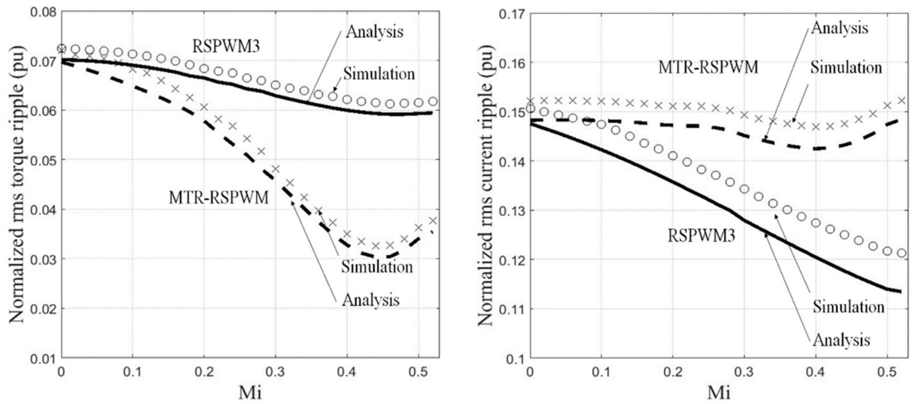

Figure 9. Analytical and simulation results: (**a**) normalized RMS torque ripple; (**b**) normalized RMS current ripple.

Figures 10a and 11a show the experimental waveforms of the phase-a current obtained by RSPWM3 and MTR-RSPWM, respectively. It is shown that for the MTR-RSPWM, the output current ripple is slightly higher than that of RSPWM3 as expected. The RMS current ripple values over a fundamental cycle according to M_i, of the RSPWM3 and the MTR-RSPWM are analyzed again later with the RMS torque ripple values.

Figures 10b and 11b show the experimental waveforms of the phase-a voltage obtained by RSPWM3 and MTR-RSPWM, respectively. For the phase-a voltage, odd pulse patterns generate $+2V_{dc}/3$ (V_1) and $-V_{dc}/3$ (V_3 and V_5), and even pulse patterns generate $+V_{dc}/3$ (V_2 and V_6) and $-2V_{dc}/3$ (V_4). Because RSPWM3 employs only one pulse pattern per sector as listed in Table 2, the values of phase voltage are fixed over a sector. On the other hand, the pulse pattern for the MTR-RSPWM is changed by the zone within a sector. The type of pulse pattern is changed from odd to even and even to odd in the odd sector (vice versa in the even sector) when the reference voltage vector crosses Zone 1, Zone 2, and Zone 3 at low M_i as shown in Figure 6. Thus, the values of phase voltage are also changed by the type of pulse pattern. However, in this case, the reference voltage vector crosses Zone 4, Zone 2, and Zone 5 at high M_i in Figure 6, because the types of pulse patterns according to the zones are same, the values of phase voltage are fixed over a sector as in RSPWM3.

Figures 10c and 11c show the experimental waveforms of the CMV obtained by the RSPWM3 and the MTR-RSPWM, respectively. The CMV also depends on the type of pulse pattern along with the phase voltage. As explained in Section 2, odd pulse patterns generate a constant CMV of $-V_{dc}/6$, and even pulse patterns generate constant CMV of $+V_{dc}/6$. At low M_i, while the CMV of RSPWM3 is fixed over a sector, the CMV of MTR-RSPWM changes its polarity twice over a sector, as shown in Figures 10c and 11c. However, the peak value of CMV is still maintained at $\pm V_{dc}/6$. Furthermore, at high M_i, the CMV of MTR-RSPWM is fixed over a sector, as it is in RSPWM3.

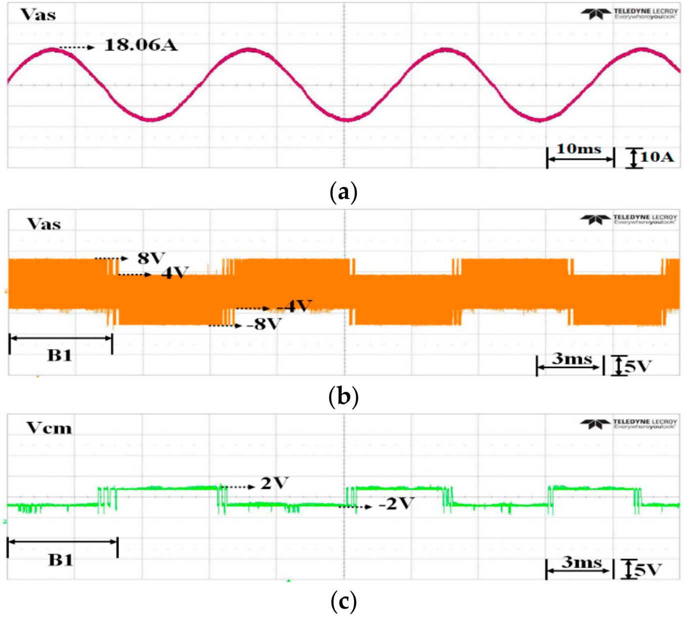

Figure 10. Experimental waveforms corresponding to the RSPWM3: (**a**) phase current; (**b**) phase voltage; (**c**) CMV.

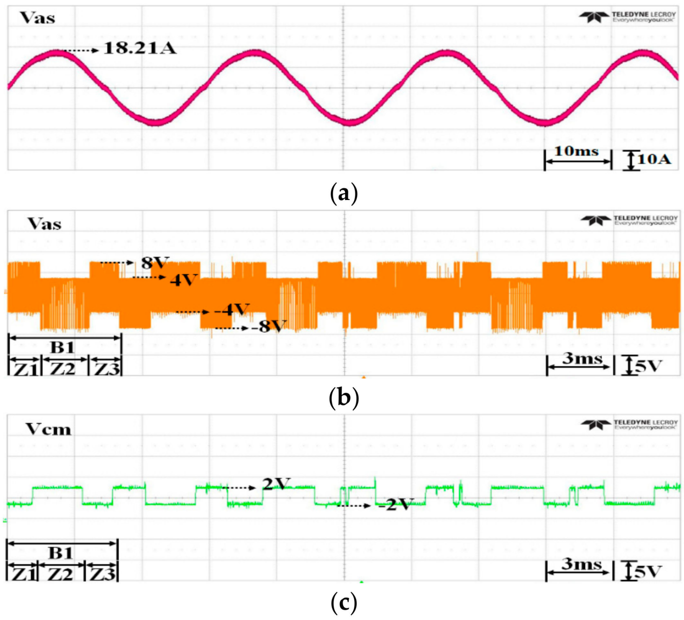

Figure 11. Experimental waveforms corresponding to the MTR-RSPWM: (**a**) phase current; (**b**) phase voltage; (**c**) CMV.

Figure 12a,b show the experimental waveforms of the output torque obtained by the RSPWM3 and the MTR-RSPWM, respectively. In the figures, the right traces are zoomed portions of the left traces when the zone is changed, where it is observed that the torque ripple closely resembles that of the q-axis current ripple shown in Figure 4. The RMS torque ripple values, over a fundamental cycle according to M_i, of the RSPWM3 and the MTR-RSPWM are shown in Figure 13a.

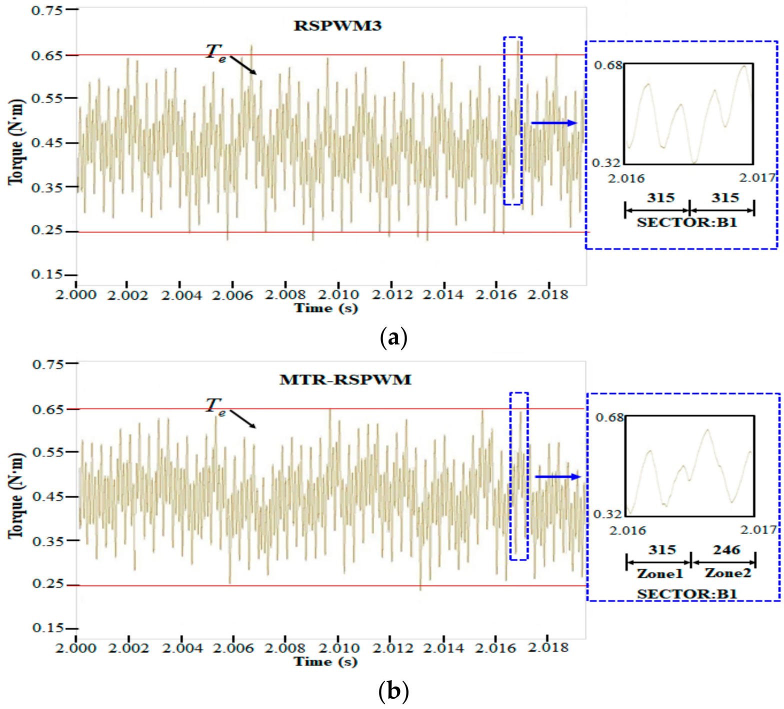

Figure 12. Experimental waveforms of output torque: (**a**) RSPWM3; (**b**) MTR-RSPWM.

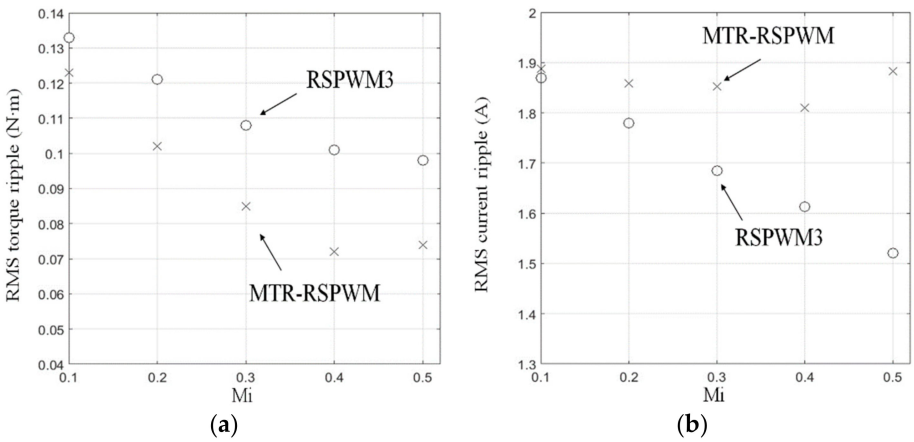

Figure 13. Experimental results: (**a**) RMS torque ripple; (**b**) RMS current ripple.

Figure 13 shows the RMS torque ripple and RMS current ripple obtained experimentally for M_i ranging from 0.1 to 0.5 in steps of 0.1. To get the instantaneous ripple, the average value is subtracted from the instantaneous value, and then the RMS values are calculated over a fundamental cycle.

Contrary to the analysis and simulation results, the experimental results are not normalized values but are practical values that include the factors (18a) and (18b), respectively. The optimum reduction is observed at $M_i = 0.4$, where the RMS torque ripple is reduced by approximately 30%. The experimental results include the effects of the device drops and dead times, the dependence of the machine parameters on frequency, depth of slots, and distortion in the distribution of magnetomotive force. Moreover, the ripple generated by the coupling that connects the BLAC motor and the load motor is also included. These factors may lead to some distortion in the experimental results of the RMS torque ripple and RMS current ripple, which in turn may result in some difference between the per cent reductions of analytical, simulation, and experimental results. Nevertheless, all these three sets of results demonstrate similar tendencies and are consistent in proving a significant reduction in the RMS torque ripple by MTR-RSPWM.

6. Conclusions

In this study, an MTR-RSPWM technique was proposed for the minimization of the RMS torque ripple under the reduced CMV conditions of three-phase VSI-fed BLAC motor drives. The RMS torque ripple over a subcycle corresponding to the six pulse patterns with reduced CMV of RSPWM was thoroughly analyzed. From the analytical results, a sector was divided by five zones, and the pulse patterns with the lowest RMS torque ripple and reduced CMV within each zone was obtained for the MTR-RSPWM. After this, the RMS torque ripple and RMS current ripple over a fundamental cycle of the RSPWM3 and MTR-RSPWM were evaluated and compared through analysis, simulation, and experiments. From the results, it is confirmed that the MTR-RSPWM significantly reduces the RMS torque ripple under reduced CMV conditions at the expense of an increase in the RMS current ripple, compared to the RSPWM3.

Author Contributions: Conceptualization, methodology, and formal analysis, J.B.; experimental validation, J.B. and S.Y.; writing original draft, J.B., D.K., and C.K.; resources and supervision, J.Y. All authors have read and agreed to the original version of the manuscript.

Funding: This research received no external funding.

Conflicts of Interest: The authors declare no conflict of interest.

References

1. Holtz, J. Pulsewidth Modulation-A Survey. *IEEE Trans. Ind. Electron.* **1992**, *39*, 410–420. [CrossRef]
2. Kazmierkowski, M.P.; Malesani, L. Current Control Techniques for Three-Phase Voltage-Source PWM Converters: A Survey. *IEEE Trans. Ind. Electron.* **1998**, *45*, 691–703. [CrossRef]
3. Casadei, D.; Serra, G.; Tani, A.; Zarri, L. Theoretical and experimental analysis for the RMS current ripple minimization in induction motor drives controlled by SVM technique. *IEEE Trans. Ind. Electron.* **2004**, *51*, 1056–1065. [CrossRef]
4. Krishnamurthy, H.; Narayanan, G.; Ayyanar, R.; Ranganathan, V.T. Design of Space Vector-Based Hybrid PWM Techniques for Reduced Current Ripple. In Proceedings of the 2003 IEEE Applied Power Electronics Conference and Exposition, Miami, FL, USA, 9–13 February 2003; pp. 1614–1627.
5. Narayanan, G.; Zhao, D.; Krishnamurthy, H.K.; Ayyanar, R.; Ranganathan, V.T. Space Vector Based Hybrid PWM Techniques for Reduced Current Ripple. *IEEE Trans. Ind. Electron.* **2008**, *55*, 1614–1627. [CrossRef]
6. Basu, K.; Siva Prasad, J.S.; Narayanan, G. Minimization of Torque Ripple in PWM AC Drives. *IEEE Trans. Ind. Electron.* **2009**, *56*, 553–558. [CrossRef]
7. Basu, K.; Siva Prasad, J.S.; Narayanan, G.; Krishnamurthy, H.K.; Ayyanar, R. Reduction of Torque Ripple in Induction Motor Drives Using an Advanced Hybrid PWM Technique. *IEEE Trans. Ind. Electron.* **2010**, *57*, 2085–2091. [CrossRef]
8. Sekhar, K.R.; Srinivas, S. Torque ripple reduction PWMs for a single DC source powered dual-inverter fed open-end winding induction motor drive. *IET Trans. Power Electron.* **2018**, *11*, 43–51. [CrossRef]
9. Cho, Y.; Bak, Y.; Lee, K.-B. Torque-Ripple Reduction and Fast Torque Response Strategy for Predictive Torque Control of Induction Motors. *IEEE Trans. Power Electron.* **2018**, *33*, 2458–2470. [CrossRef]
10. Bak, Y.; Jang, Y.; Lee, K.-B. Torque Predictive Control for Permanent Magnet Synchronous Motor Drives Using Indirect Matrix Converter. *J. Power Electron.* **2019**, *19*, 1536–1543.
11. Wu, W.; Sun, Y.; Lin, Z.; He, Y.; Huang, M.; Blaabjerg, F.; Chung, H.S. A Modified LLCL Filter with the Reduced Conducted EMI Noise. *IEEE Trans. Power Electron.* **2014**, *29*, 3393–3402. [CrossRef]
12. Guzman, R.; Vicuna, L.G.; Morales, J.; Castilla, M.; Miret, J. Model-Based Active Damping Control for Three-Phase Voltage Source Inverters with LCL Filter. *IEEE Trans. Power Electron.* **2017**, *32*, 5637–5650. [CrossRef]
13. Morris, C.T.; Han, D.; Sarlioglu, B. Reduction of Common Mode Voltage and Conducted EMI Through Three-Phase Inverter Topology. *IEEE Trans. Power Electron.* **2017**, *32*, 1720–1724. [CrossRef]
14. Han, D.; Morris, C.T.; Sarlioglu, B. Common-Mode Voltage Cancellation in PWM Motor Drives with Balanced Inverter Topology. *IEEE Trans. Ind. Electron.* **2017**, *64*, 2683–2688. [CrossRef]

15. Yun, S.W.; Baik, J.H.; Kim, D.S.; Yoo, J.Y. A New Active Zero State PWM Algorithm for Reducing the Number of Switchings. *J. Power Electron.* **2017**, *17*, 88–95. [CrossRef]
16. Baik, J.H.; Yun, S.W.; Kim, D.S.; Kwon, C.K.; Yoo, J.Y. EMI Noise Reduction with New Active Zero State PWM for Integrated Dynamic Brake Systems. *J. Power Electron.* **2018**, *18*, 923–930.
17. Cacciato, M.; Consoli, A.; Scarcella, G.; Testa, A. Reduction of Common-Mode Currents in PWM Inverter Motor Drives. *IEEE Trans. Ind. Appl.* **1999**, *35*, 469–476. [CrossRef]
18. Un, E.; Hava, A.M. A Near-State PWM Method With Reduced Switching Losses and Reduced Common-Mode Voltage for Three-Phase Voltage Source Inverters. *IEEE Trans. Ind. Appl.* **2009**, *45*, 782–793. [CrossRef]
19. Hava, A.M.; Un, E. Performance Analysis of Reduced Common-Mode Voltage PWM Methods and Comparison With Standard PWM Methods for Three-Phase Voltage Source Inverters. *IEEE Trans. Power Electron.* **2009**, *24*, 241–252. [CrossRef]
20. Chen, H.; Zhao, H. Review on pulse-width modulation strategies for common-mode voltage reduction in three-phase voltage-source inverters. *IET Trans. Power Electron.* **2016**, *9*, 2611–2612. [CrossRef]
21. Nguyen, T.-K.T.; Nguyen, N.-V. An Efficient Four-State Zero Common-Mode Voltage PWM Scheme with Reduced Current Distortion for a Three-Level Inverter. *IEEE Trans. Ind. Electron.* **2018**, *65*, 1021–1030. [CrossRef]
22. Kalaiselvi, J.; Srinivas, S. Bearing Currents and Shaft Voltage Reduction in Dual-Inverter-Fed Open-End Winding Induction Motor With Reduced CMV PWM Methods. *IEEE Trans. Ind. Electron.* **2015**, *62*, 144–152. [CrossRef]
23. Do, D.-T.; Nguyen, M.-K.; Ngo, V.-T.; Quach, T.-H.; Tran, V.-T. Common Mode Voltage Elimination for Quasi-Switch Boost T-Type Inverter Based on SVM Technique. *Electronics* **2020**, *9*, 76. [CrossRef]
24. Rzasa, J. An Alternative Carrier-Based Implementation of Space Vector Modulation to Eliminate Common Mode Voltage in a Multilevel Matrix Converter. *Electronics* **2019**, *8*, 190. [CrossRef]
25. Jun, E.-S.; Park, S.-Y.; Kwak, S. A Comprehensive Double-Vector Approach to Alleviate Common-Mode Voltage in Three-Phase Voltage-Source Inverters with a Predictive Control Algorithm. *Electronics* **2019**, *8*, 872. [CrossRef]
26. Mahmoudi, H.; Aleenejad, M.; Ahmadi, R. Torque Ripple Minimization for a Permanent Magnet Synchronous Motor Using a Modified Quasi-Z-Source Inverter. *IEEE Trans. Power Electron.* **2019**, *34*, 3819–3830. [CrossRef]
27. Cai, H.; Wang, H.; Li, M.; Shen, S.; Feng, Y.; Zheng, J. Torque Ripple Reduction for Switched Reluctance Motor with Optimized PWM Control Strategy. *Energies* **2018**, *11*, 3215. [CrossRef]